Incidence of B-cell Malignancies in Patients with Lung Cancer Receiving PD-1 Blockade Therapy

Toshifumi Ninomiya[1,2], Caiyang Fang[1], Hirofumi Hamano[3], Teruya Morinaga[1], Wenhao Zhou[1,4,5], Toshihiro Koyama[6], Sakura Miki[1], Li Zhu[1], Yusuke Naoi[7], Daisuke Ennishi[7], Tomoya Katsuta[8], Kadoaki Ohashi[9], Shin Morizane[10], Tomoka Ohki-Ikeda[11], Tatsuya Nishi[1,7], Youki Ueda[1], Takamasa Ishino[1], Yoshinobu Maeda[7], Isamu Okamoto[2], Yoshito Zamami[3], Joji Nagasaki[1,12], and Yosuke Togashi[1,9,13]

ABSTRACT

Purpose: Many patients with various cancer types have received immune checkpoint inhibitors (ICI) worldwide since their approval, and novel unexpected complications from their long-term use are apparent. We identified some cases of B-cell lymphoma occurring during PD-1 blockade therapy as such unexpected complications. In this study, we aimed to evaluate the incidence of hematologic malignancies in patients with lung cancer receiving PD-1 blockade therapy and to elucidate the mechanisms underlying the progression of these malignancies.

Experimental Design: We performed IHC staining on the clinical samples from patients with B-cell lymphoma that developed during PD-1 blockade therapy and analyzed large-scale real-world datasets. We further investigated the underlying mechanisms through *in vitro* and *in vivo* experiments.

Results: A higher incidence of B-cell malignancies has been observed in patients with lung cancer treated with PD-1 blockade therapies based on large-scale real-world data analyses ($n = 15{,}670$). The identified lymphomas had a large amount of $CD4^+$ T follicular helper (T_{FH}) cell infiltration. In addition, PD-1 blockade activated $PD\text{-}1^+$ T_{FH} cells, which promoted lymphoma proliferation via the IL4/IL4R, IL21/IL21R, and CD40L/CD40 axes. Notably, the lymphomas exhibited high expression of IL4R, IL21R, and CD40.

Conclusions: Our findings highlight the need for careful monitoring and consideration of the potential B-cell malignancy complications in clinical settings in which ICIs are used.

Introduction

Cancer remains one of the leading causes of mortality worldwide, with more than 10 million deaths reported annually (1). In addition to cytotoxic chemotherapy and molecularly targeted therapy, cancer immunotherapy has rapidly advanced over the past decade. Immune checkpoint inhibitors (ICI), such as anti–PD-1/PD-L1 and anti–CTLA-4 antibodies, have been used in the treatment of a wide range of cancers, including lung cancer (2, 3), melanoma (4), and renal cell carcinoma (5), demonstrating favorable therapeutic outcomes (2–5). Notably, some patients treated with ICIs reportedly achieve a durable response. However, novel unexpected complications can occur in such patients, and attention should be paid to them.

The ICIs exhibit efficacy by reactivating T cells that directly attack tumors (6, 7). Tumor cells generally express major histocompatibility complex class I, which is recognized by $CD8^+$ T cells (8). Thus, $CD8^+$ T cells play a crucial role in antitumor immunity and ICI efficacy (8, 9). The importance of $CD4^+$ T cells in antitumor immunity has also been documented (10–12). $CD4^+$ T cells perform a wide variety of functions and are well-known for their role as T-helper cells. Among these T-helper cells, $CD4^+$ T follicular helper (T_{FH}) cells have recently garnered significant attention because of their crucial role in supporting the formation and maintenance of germinal centers (GC) in lymphoid tissues (13). T_{FH} cells are originally involved in B-cell maturation and GC support via costimulatory signals and cytokines (13, 14). In addition, T_{FH} cells are beneficial for generating memory B cells and antibodies via IL4 and IL21 in lymphoid tissues (14–16). These B cells produce antibodies and act as antigen-presenting cells (APC; ref. 17). Given these functions, it is reasonable to assume that T_{FH} cells play a positive role in antitumor immunity.

[1]Department of Tumor Microenvironment, Faculty of Medicine, Dentistry and Pharmaceutical Sciences, Okayama University, Okayama, Japan. [2]Department of Respiratory Medicine, Graduate School of Medical Sciences, Kyushu University, Fukuoka, Japan. [3]Department of Pharmacy, Okayama University Hospital, Okayama University, Okayama, Japan. [4]Department of Immunology, Nagoya University Graduate School of Medicine, Nagoya, Japan. [5]Department of Urology Surgery, Affiliated Hospital of North Sichuan Medical College, Nanchong, China. [6]Department of Pharmaceutical Data Science, Graduate School of Medicine, Dentistry, and Pharmaceutical Sciences, Okayama University, Okayama, Japan. [7]Department of Hematology, Oncology and Respiratory Medicine, Faculty of Medicine, Dentistry and Pharmaceutical Sciences, Okayama University, Okayama, Japan. [8]Department of Respiratory Medicine, Ehime Prefectural Central Hospital, Matsuyama, Japan. [9]Department of Respiratory Medicine, Okayama University Hospital, Okayama University, Okayama, Japan. [10]Department of Dermatology, Faculty of Medicine, Dentistry and Pharmaceutical Sciences, Okayama University, Okayama, Japan. [11]Department of Pathology, Okayama University Hospital, Okayama University, Okayama, Japan. [12]Department of Hematology, Osaka Metropolitan University, Graduate School of Medicine, Osaka, Japan. [13]Kindai University Faculty of Medicine, Osaka, Japan.

T. Ninomiya and C. Fang contributed equally to this article as co-first authors.

Corresponding Authors: Yosuke Togashi, Department of Tumor Microenvironment, Faculty of Medicine, Dentistry and Pharmaceutical Sciences, Okayama University, Okayama 700–8558, Japan. E-mail: ytogashi@okayama-u.ac.jp, ytogashi1584@gmail.com; and Joji Nagasaki, pjuk18gs@okayama-u.ac.jp, george.nagasaki.1985@gmail.com

Clin Cancer Res 2026;XX:XX–XX

doi: 10.1158/1078-0432.CCR-25-3406

Translational Relevance

Immune checkpoint inhibitors (ICI), particularly PD-1 blockade therapies, have become standard treatments for various cancer types, but unexpected complications are emerging with long-term use. In this study, we identified cases of B-cell lymphoma that developed during PD-1 blockade and confirmed, through large-scale real-world datasets, that patients receiving ICIs have an increased incidence of lymphoma. Mechanistically, PD-1 blockade activates PD-1$^+$ T follicular helper cells, which promote lymphoma progression through IL4, IL21, and CD40 signaling pathways. These findings underscore the importance of monitoring for hematologic complications in patients undergoing ICI therapy. This has significant implications for both clinical practice and research, highlighting the need for vigilant surveillance and the development of strategies to mitigate these risks.

The T_{FH} cells are distinguished from others by the high expression of CXCR5 and PD-1 (13, 18–20). As PD-1 suppresses T_{FH} cells, PD-1 blockade activates PD-1$^+$ T_{FH} cells (11, 20). Accordingly, T_{FH} cells activated by PD-1 blockade reportedly contribute to antitumor immunity by helping CD8$^+$ T cells (11, 21–23). T_{FH} cell infiltration is a good prognostic factor in patients with solid tumors treated with ICIs (23–26). However, given that B-cell malignancies originate from B cells, T_{FH} cells can support malignant cells via ligands and cytokines (26–31). Notably, T_{FH} cell infiltration is recognized as a poor prognostic factor for B-cell malignancies, in contrast to solid tumors (26–31).

In this study, we found that patients with lung cancer developed B-cell malignancies with extensive T_{FH} cell infiltration during PD-1 blockade therapy. Therefore, we hypothesized that PD-1$^+$ T_{FH} cells activated by PD-1 blockade might promote B-cell malignancy proliferation, apart from having a positive effect on CD8$^+$ T cells, and investigated the role of T_{FH} cells. Additionally, the incidence of hematologic malignancies in patients with lung cancer who received systemic chemotherapy, including PD-1 blockade therapy, was evaluated using large-scale real-world datasets. Our findings provide novel insights into potential B-cell malignancy complications in clinical settings in which ICIs are used.

Materials and Methods

Patients

Lymphoma specimens from two patients who developed malignant lymphoma during PD-1 blockade therapy were used for IHC analysis (**Fig. 1**; Supplementary Table S1). In addition, lymphoma specimens from 10 patients diagnosed with B-cell malignant lymphoma, including follicular lymphoma (FL) and diffuse large B-cell lymphoma (DLBCL), at Okayama University Hospital between 2021 and 2024 were also used for IHC analysis (Supplementary Table S1). The study protocol was approved by the Institutional Review Board and Ethics Committee of Okayama University Hospital.

IHC

Paraffin-embedded sections of the surgical specimen were similarly cut into 3-μm slices, deparaffinized, and rehydrated. Antigen retrieval was performed using citrate buffer (pH 6.0; LSI Medience Corporation; cat. #2-3106-08) at 121°C for 20 minutes. After blocking endogenous peroxidase activity with 3% H_2O_2, the tissues were treated with 3% bovine serum albumin (Nacalai Tesque; cat. #01860-07) in phosphate-buffered saline (PBS) to block nonspecific reactions in a humid box at room temperature (RT). Anti-human CD40 antibody (Abcam; clone EPR20540; cat. #ab213205), anti-human IL4Rα antibody (R&D Systems; clone 25463; cat. #MAB230, RRID: AB_2126871), or anti-human IL21R antibody (Proteintech; clone 1D1C2; cat. #66319-1-Ig, RRID: AB_2881700) diluted in 3% BSA was added to tissues and incubated overnight in a humidity box at 4°C. The control slides were incubated with only 3% BSA. The tissues were washed and incubated with SignalStain Boost IHC Detection Reagent (horseradish peroxidase, mouse or rabbit; Cell Signaling Technology; cat. #8125 or cat. #8114) for 30 minutes in a humidity box at RT. After washing, 3,3′-diaminobenzidine (DAB) staining was performed using the SignalStain DAB Substrate Kit (Cell Signaling Technology; cat. #8059). Counterstaining was performed with hematoxylin, and the tissues were mounted.

For multicolor IHC, EDTA buffer pH 8.0 was used at 121°C for 20 minutes following the antigen retrieval method. Subsequently, permeabilization was performed by treating the samples with 0.2% Tween-20 dissolved in PBS for 10 minutes. After blocking nonspecific reactions, the tissues were incubated overnight with the anti-human CD4 polyclonal antibody (R&D Systems; cat. #AF-379-NA, RRID: AB_354469), anti-human CD8 antibody (Cell Signaling Technology; clone D8A8Y, cat. #85336, RRID: AB_2800052), anti-human FOXP3 antibody (Abcam; clone 236A/E7, cat. #ab20034, RRID: AB_445284), anti-human Bcl-6 antibody (Cell Signaling Technology; clone E5I8I, cat. #89369, RRID: AB_2800138), and anti-human T-bet antibody (Thermo Fisher Scientific; clone 4B10, cat. #14-5825-82, RRID: AB_763634) diluted in 3% BSA at 4°C and washed. The secondary antibodies, donkey anti-mouse IgG H&L Alexa Fluor 488 (Abcam; cat. #ab150105, RRID: AB_2732856), anti-rabbit IgG H&L Alexa Fluor 555 (Abcam; cat. #ab150078, RRID: AB_2722519), and donkey anti-goat IgG H&L Alexa Fluor 647 (Abcam; cat. #ab150131, RRID: AB_2732857), were diluted with 3% BSA and reacted with the tissues at RT. The samples were washed and sealed using the TrueVIEW Autofluorescence Quenching Kit with DAPI (Vector Laboratories; cat. #SP-8500-15). All images were captured using an all-in-one fluorescence microscope (BZ-X700; Central Research Laboratory, Okayama University Medical School, Japan).

Dataset

The initial data were collected from the Medical Data Vision (MDV) database (Medical Data Vision Co., Ltd.), which covers 485 acute care institutions in Japan. The second and third data were collected from the World Health Organization (WHO) pharmacovigilance database and the WHO Mortality Database, respectively. All databases were extracted using Navicat for SQLite (version 16.3.7, PremiumSoft) and Microsoft Access software from Microsoft 365 (Office; Microsoft Corporation).

Data analysis

First, the MDV analysis utilized data from January 2010 to December 2021 as the study period, confirming that the health insurance claims database recorded 1,040,184 prescriptions classified as antineoplastic agents under the Anatomical Therapeutic Chemical classification system code L01. The analysis targeted patients ≥18 years of age with lung cancer and divided them into two groups. The platinum-based chemotherapy (Pt) + ICI group included patients who

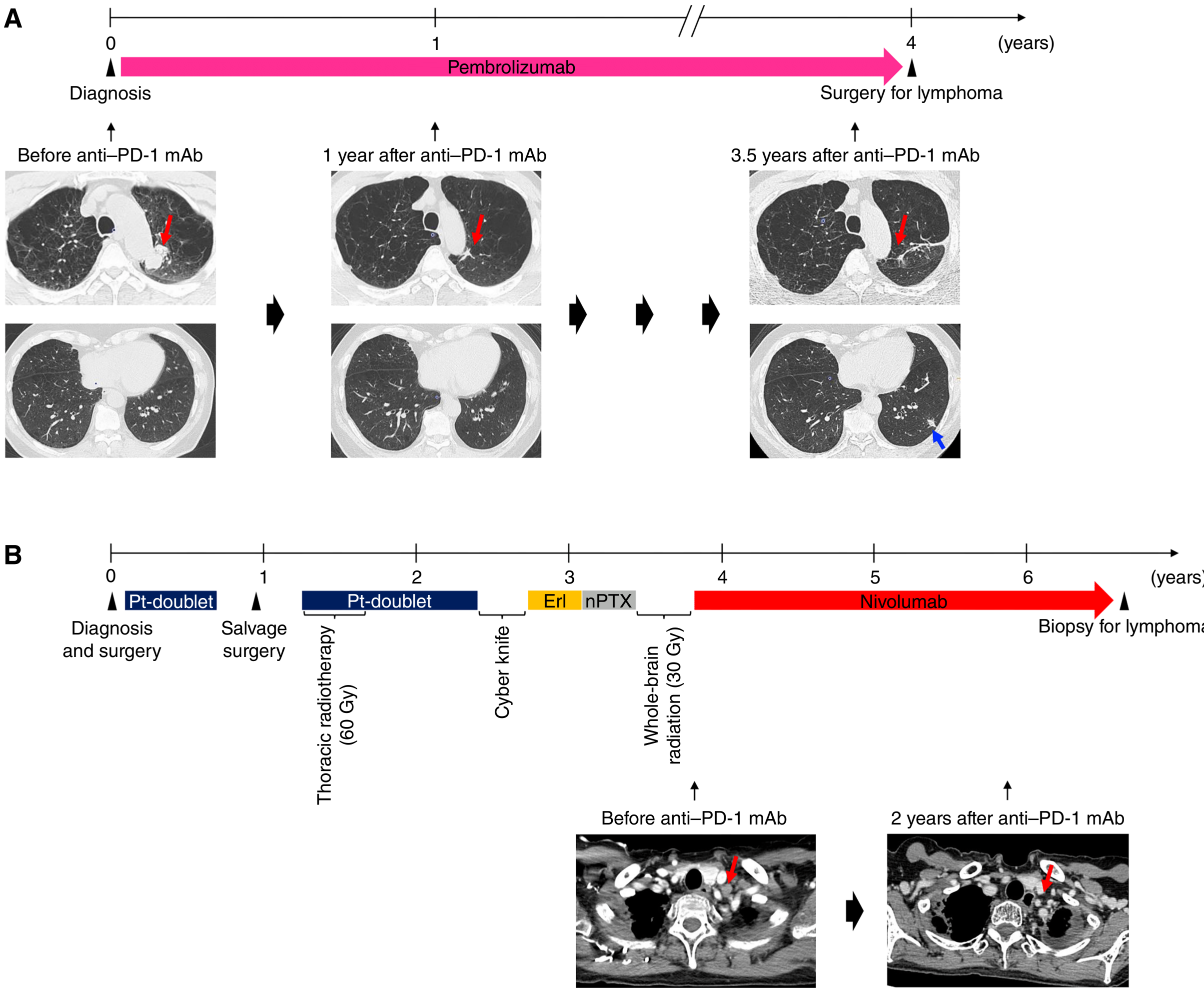

Figure 1.

Clinical courses. **A,** Case 1. Case 1 is a male in his late 60s with NSCLC who developed MALT lymphoma during pembrolizumab monotherapy. After the diagnosis of stage IV NSCLC, he received pembrolizumab monotherapy as the first-line treatment. He achieved a partial response and continued the therapy afterward (red arrows). Before and during the treatment, he never received any other chemotherapies or radiotherapies. A pulmonary nodule was found 3.5 years later, in which the size increased gradually even though the other lesions were stable during pembrolizumab monotherapy (a blue arrow). He received surgery for the increased pulmonary nodule and was diagnosed with lymphoma. **B,** Case 2. Case 2 is a female in her late 50s with NSCLC who developed primary cutaneous follicle center lymphoma during nivolumab monotherapy. She received heavy treatment for NSCLC. Eventually, nivolumab monotherapy started as the fifth-line treatment 3.5 years after diagnosis, resulting in a complete response (red arrows). However, 2.5 years after the initiation of nivolumab, she developed cervical erythema during nivolumab monotherapy and was diagnosed with lymphoma. Erl, erlotinib; nPTX, nanoparticle albumin–bound paclitaxel; Pt, platinum.

received initial prescriptions of ICIs and platinum-based anticancer agents [Pt: carboplatin (CBDCA) or cisplatin (CDDP)] between January 2017 and December 2021. As a control group, patients who received their initial prescription of platinum-based chemotherapy alone between January 2010 and December 2014 were included because ICIs were not approved as the first-line therapy during this period in Japan. Patients were excluded if they had no diagnosis of lung cancer before the index date, had been diagnosed with cancers other than lung cancer before the index date, had been prescribed antineoplastic agents before the index date, had undergone radiotherapy before the index date, or had a lookback period of less than 60 days. Additionally, those who had been prescribed EGFR or ALK tyrosine kinase inhibitors were excluded because few patients with *EGFR*-mutated or *ALK*-fused lung cancer received ICIs as the first-line therapy. The list of drugs used in this study is provided in Supplementary Table S2, and the patient selection criteria are illustrated in Supplementary Fig. S1. Diagnoses of lung cancer and hematologic events were identified based on ICD-10 codes, as detailed in Supplementary Table S3. The definitions of radiotherapy are presented in Supplementary Table S4. The follow-up period for hematologic event outcomes was set to 1 year because nivolumab has been approved as the second-line or later therapy in Japan since December 2015. To assess the robustness of the primary survival analysis and competing risk analysis results, sensitivity analyses were performed through subgroup stratification by age (<65 or ≥65 years), sex, smoking status (Brinkman index = 0 or ≥1), and platinum agent type (carboplatin or cisplatin). Relative risks and 95% confidence intervals were calculated for each subgroup.

Second, data from the WHO pharmacovigilance database from January 2017 to December 2023, the maximum duration available, were analyzed. Supplementary Figure S2 presents a flowchart outlining the patient selection process. This analysis was guided by statistical algorithms developed by the WHO collaborating center. These algorithms have formed the foundation of our ongoing efforts to explore this dataset and identify medications that may pose risks. Duplicate reports were identified in VigiBase using an automated VigiMatch algorithm (32). This method was crucial in improving the precision of our analysis, beginning with the removal of duplicate entries to maintain data integrity. For any suspected duplicates, the report with the highest VigiGrade completeness score was flagged for further review (33). Lymphoma cases are defined as any individual case safety report (ICSR) with a reported term included in the following High-Level Group Terms of the Medical Dictionary for Regulatory Activities/J (version 26.0; International Glossary of Pharmaceutical Terms of the International Council for Harmonization of Technical Requirements for Pharmaceuticals for Human Use): lymphomas Hodgkin disease, lymphomas not elsewhere classified, lymphomas non-Hodgkin B cell, lymphomas non-Hodgkin T-cell, and lymphomas non-Hodgkin unspecified. ICSRs that included an ICI used to treat lymphoma were excluded because their drug causality was doubtful.

Finally, detailed data from the WHO Mortality Database on the crude incidence rate and age-standardized incidence rate of lymphoma in Japan from 2010 to 2020 were analyzed. The diagnosis of lymphoma was defined based on ICD-9 and ICD-10 codes. The crude incidence rate was calculated using the number of lymphoma diagnoses as the numerator and the population obtained from the Japan Population Prospects database as the denominator. The age-standardized incidence rate was calculated using the world standard population as the reference for each 5-year age group to adjust for the differences in population age structure.

Cell line

The E.G7 (cat. #CRL-2113, RRID: CVCL_3505) and A20 (cat. #TIB-208, RRID: CVCL_1940) cell lines were obtained from ATCC. The cell lines were maintained in RPMI 1640 medium supplemented with 10% FBS (Thermo Fisher Scientific; cat. #A5256701). All cell lines were routinely tested and confirmed to be *Mycoplasma*-free using a PCR Mycoplasma Detection Kit (Takara Bio; cat. #6601), according to the manufacturer's instructions. Cell lines were used in experiments within 10 passages after thawing.

Reagent

Mouse IL4 (cat. #214-14) and IL21 (cat. #210-21) were purchased from PeproTech. Mouse IL6 (cat. #094-07001) was purchased from FUJIFILM Wako Pure Chemical. Soluble CD40L (sCD40L; cat. #PEP-CYT-472) was purchased from Enzo Biochem. Anti-mouse CD3 (clone 145-2C11, cat. #100359, RRID: AB_2616673), anti-mouse CD28 (clone 37.51, cat. #102116, RRID: AB_11147170), and anti-mouse PD-1 (clone: RMP1-14, cat. #114122, RRID: AB_2159165) monoclonal antibodies (mAb) were purchased from BioLegend. Anti-mouse IL4 (clone 11B11, cat. #BE0045, RRID: AB_1107707) and IL21R (clone 4A9, cat. #BE0258, RRID: AB_2687737) mAbs were purchased from BioXCell. Anti-mouse CD40 mAbs (clone: HM40-3, cat. #14-0402-82, RRID: AB_467228) were purchased from Thermo Fisher Scientific.

Construct and viral transfection

Plasmids pMSCV-*Il4r*, pMSCV-*Il21r*, and pMSCV-*Cd40* were purchased from VectorBuilder. Each vector and the pVSV-G vector (Takara Bio; cat. #S1958) were transfected into packaging cells using Lipofectamine 3000 Transfection Reagent (Thermo Fisher Scientific; cat. #L3000015). After 48 hours, the supernatant was concentrated and transduced into the cells. The expression was assessed using flow cytometry.

CD40 deletion using the CRISPR/Cas9 system

The CD40-deleted A20 cells were generated using the CRISPR/Cas9 system. Briefly, guide RNA (gRNA) sequences (5′-GTCCGT-ACTCCGCCAGTATG-3′ targeting *Cd40*) were used to edit the genomic locus. The gRNA (Thermo Fisher Scientific; cat. #A35533, CRISPR521641_SGM CD40) and Cas9 protein (Thermo Fisher Scientific; cat. #A36497) were transfected into A20 cells via electroporation (Bio-Rad; cat. #1652660J1). The expression was assessed via flow cytometry.

In vitro T_{FH} cell analysis

To induce T_{FH} cells, we used a previously reported protocol (34). Briefly, naïve $CD4^+$ T cells were isolated from splenocytes of C57BL/6 mice using the MojoSort Mouse CD4 Naïve T Cell Isolation Kit (cat. #480039, BioLegend), according to the manufacturer's instructions. Purified naïve $CD4^+$ T cells were initially stimulated with gamma-irradiated APCs (T cell–depleted splenocytes) in the presence of anti-CD3 mAb (2 μg/mL; BioLegend) and cultured in a medium supplemented with IL6 (50 ng/mL) and IL21 (50 ng/mL) for 4 days. Anti–PD-1 mAb (5 μg/mL) was added on day 4 of the culture in the presence of gamma-irradiated APCs. After 24 hours with or without anti–PD-1 mAb (5 μg/mL), T_{FH} cells ($PD\text{-}1^+CXCR5^+FOXP3^-CD4^+$ T cells) were analyzed using flow cytometry. *In vitro* experiments were performed in triplicate independently using three samples per group.

In vitro proliferation assay

For standard proliferation assays, 5×10^4 cells were seeded in a 96-well plate and treated with IL4, IL21, or sCD40L at the indicated concentrations, with or without anti-IL4, IL21R, or CD40 mAb. After 48 hours, cell proliferation was assessed using the Cell Counting Kit-8 (Fujifilm; cat. #343-07623). Carboxyfluorescein succinimidyl ester (CFSE) analysis was also performed to evaluate cell proliferation. Briefly, E.G7 cells were stained with CFSE using the CellTrace CFSE Cell Proliferation Kit (Thermo Fisher Scientific; cat. #C34570). Stained cells were cultured with IL4 or IL21 at the indicated concentrations, with or without anti-IL4 or IL21R mAb. Cells were analyzed using flow cytometry 48 hours after the initiation of culture, and the undivided peak was defined based on the control (0 hours), and proliferation was quantified using the proliferation index calculated via FlowJo. In addition, $CD62L^+CD25^-CD4^+$ T cells (naïve $CD4^+$ T cells) were sorted from mouse splenocytes, and $PD\text{-}1^+CXCR5^+CD25^-CD4^+$ T cells (T_{FH} cells) were sorted from mouse splenocytes cultured under the T_{FH} induction condition as described above, using a FACSAria Cell Sorter at the Central Research Laboratory, Okayama University Medical School. Each sorted fraction was subsequently cocultured with E.G7 cells in transwell plates with a pore size of 0.4 μm (Corning; cat. #3381) with or without anti-IL4 (10 μg/mL) and/or IL21R (10 μg/mL) mAbs. After 48 hours, cell proliferation was assessed using the CCK-8 assay. *In vitro* experiments were performed in triplicate independently using three samples per group.

Western blotting

Following treatment with IL4 (100 ng/mL), IL21 (200 ng/mL), or sCD40L (200 ng/mL), either alone or in combination with anti-IL4 mAb (10 μg/mL), anti-IL21R mAb (10 μg/mL), or anti-CD40 mAb (1 μg/mL) for 30 minutes, cells were collected, washed with PBS, and suspended in lysis buffer containing 1% SDS (Nacalai Tesque; cat. #30562-04), 10 mmol/L of Tris–HCl (Nacalai Tesque; cat. #32739-31), protease inhibitor cocktail (Cell Signaling Technology; cat. #5871), and phosphatase inhibitor cocktail (Cell Signaling Technology; cat. #5870). Equal amounts of proteins from whole-cell lysates were separated via SDS-PAGE and blotted onto a transfer membrane (Millipore; cat. #IPVH00010). After blocking, the membranes were probed with primary antibodies. Antibodies specific for STAT3 (clone D3Z2G, cat. #12640, RRID: AB_2629499), pSTAT3 (Tyr705; clone D3A7, cat. #9145, RRID: AB_2491009), STAT6 (clone D3H4, cat. #5397, RRID: AB_11220421), pSTAT6 (Tyr641; clone D8S9Y, cat. #56554, RRID: AB_2799514), Akt (cat. #9272, RRID: AB_329827), and pAkt (Ser473; cat. #9271, RRID: AB_329825) were purchased from Cell Signaling Technology. The anti–β-actin antibody (clone AC-15, cat. #A1978, RRID: AB_476692) was purchased from Merck and used as a loading control. After rinsing twice with TBS, the membrane was incubated with a horseradish peroxidase–conjugated secondary antibody (Cell Signaling Technology; cat. #7074 or cat. #7076), washed, and visualized using an ECL detection system (PerkinElmer; cat. #275-20471) and a ChemiDoc imaging system (Bio-Rad).

Mouse model

The following mouse strains were used in this study: Female C57BL/6J and BALB/c mice were purchased from SLC Japan. B6.Cg-Tg(Cd4-cre)1Cwi/BfluJ mice (*Cd4*^{cre}; IMSR_JAX:022071) and B6.129S(FVB)-Bcl6tm1.1Dent/J mice (*Bcl6*^{fl}; IMSR_JAX: 023727) were purchased from Jackson Laboratories. All mice were maintained under pathogen-free conditions in the animal facilities. All animal experiments were approved by the Animal Care and Use Committee of Okayama University in accordance with the Animal Welfare and Management Act of Japan.

The E.G7 or A20 cells (5×10^6 cells) were injected subcutaneously, and the tumor volume was monitored twice a week. The means of the long and short tumor diameters were used to generate tumor growth curves. The mice were grouped on day 7, and anti–PD-1 mAb (200 μg/mouse) or control mAb was administered intraperitoneally three times every 3 days. The tumors were harvested on day 14 for tumor-infiltrating lymphocyte (TIL) and tumor-draining lymph node (dLN) analysis. *In vivo* experiments were performed at least twice.

Flow cytometry analysis

The cells were washed with PBS (Wako Pure Chemical Corporation; cat. #048-29805) containing 2% FBS and stained with surface antibodies. Intracellular staining was performed with specific antibodies and the FOXP3/Transcription Factor Staining Buffer Set (Thermo Fisher Scientific; cat. #00-5523-00), according to the manufacturer's instructions. For intracellular cytokine staining, cells were stimulated for 6 hours with anti-CD3 (5 μg/mL) and CD28 (2 μg/mL) mAbs, along with GolgiPlug reagent (BD Biosciences; cat. #555029). The samples were assessed using a BD FACSFortessa instrument (BD Biosciences) and FlowJo software (BD Biosciences; ref. 9). The antibodies used are summarized in Supplementary Table S5 and were diluted according to the manufacturer's instructions. The gating strategies are shown in Supplementary Figs. S3 and S4. About the distinction among subsets, we defined gates using isotype controls.

Statistical analysis

GraphPad Prism 8 (GraphPad Software), R software (version 4.1.2, R Foundation for Statistical Computing), Joinpoint Regression Program (version 5.1.0.0, National Cancer Institute), and Python (version 3.9.7, Python Software Foundation) were used for statistical analyses. The relationships of continuous variables between or among groups were compared using a *t* test or one-way ANOVA, respectively. The relationships between tumor volume curves were compared using two-way ANOVA. For multiple testing, a Bonferroni correction was used.

The analysis of hematologic events (lymphoma, leukemia, and multiple myeloma) between the treatment groups was conducted using event time–based incidence distribution and competing risk analyses. The censoring criteria were defined as follows: (i) 365 days after the index date (day 0, defined as the initial prescription date of the Pt); (ii) the observation end date in the database, which was either the maximum date available in the database or the last confirmed month of medical records for individual patients; (iii) the earliest date of radiotherapy billing after day 0; and (iv) the date of death. The log-rank test was used to compare the event time–based incidence distributions between treatment groups. The Gray test was used to analyze cumulative incidence functions considering competing risks (death and radiotherapy; refs. 35, 36). This methodologic approach evaluated treatment effects on hematologic events from event time–based incidence and competing risk perspectives. Smoothed curves of lymphoma incidence rates in Japan during the study period were created using locally estimated scatterplot smoothing weighted by population size to understand long-term trends. Statistical significance was determined using *P* values with a threshold set at 0.05.

Results

Two cases with lung cancer had malignant lymphoma during PD-1 blockade therapies

We identified two individuals with lung cancer who developed malignant lymphoma during PD-1 blockade therapy; their clinical courses are summarized in **Fig. 1** and Supplementary Table S1. Case 1 involved a male patient in his late 60s with non–small cell lung cancer (NSCLC) who developed extranodal marginal zone lymphoma of the mucosa-associated lymphoid tissue (MALT lymphoma) during pembrolizumab monotherapy. After the diagnosis of stage IV NSCLC, he received pembrolizumab monotherapy as the first-line treatment. He achieved a partial response and continued the therapy. Before and during the treatment, the patient did not receive any other chemotherapy or radiotherapy. A pulmonary nodule was found 3.5 years later, the size of which increased gradually, although the other lesions were stable during pembrolizumab monotherapy (**Fig. 1**). Four years later, the patient underwent surgical resection of the nodule, and the pathology showed MALT lymphoma, that is, lymphoepithelial lesions in hematoxylin and eosin (H&E) staining and IHC staining for $CD3^-$, $CD10^-$, $CD20^+$, and BCL-2^+ (**Fig. 2A**). Case 2 involved a female in her late 50s with NSCLC, who developed primary cutaneous follicle center lymphoma during nivolumab monotherapy. She received intensive treatment for NSCLC (surgical resection, platinum doublets, erlotinib, nab-paclitaxel, thoracic radiotherapy, and whole-brain radiation). Eventually, nivolumab monotherapy was initiated as the fifth-line treatment 3.5 years after diagnosis, resulting in a complete response.

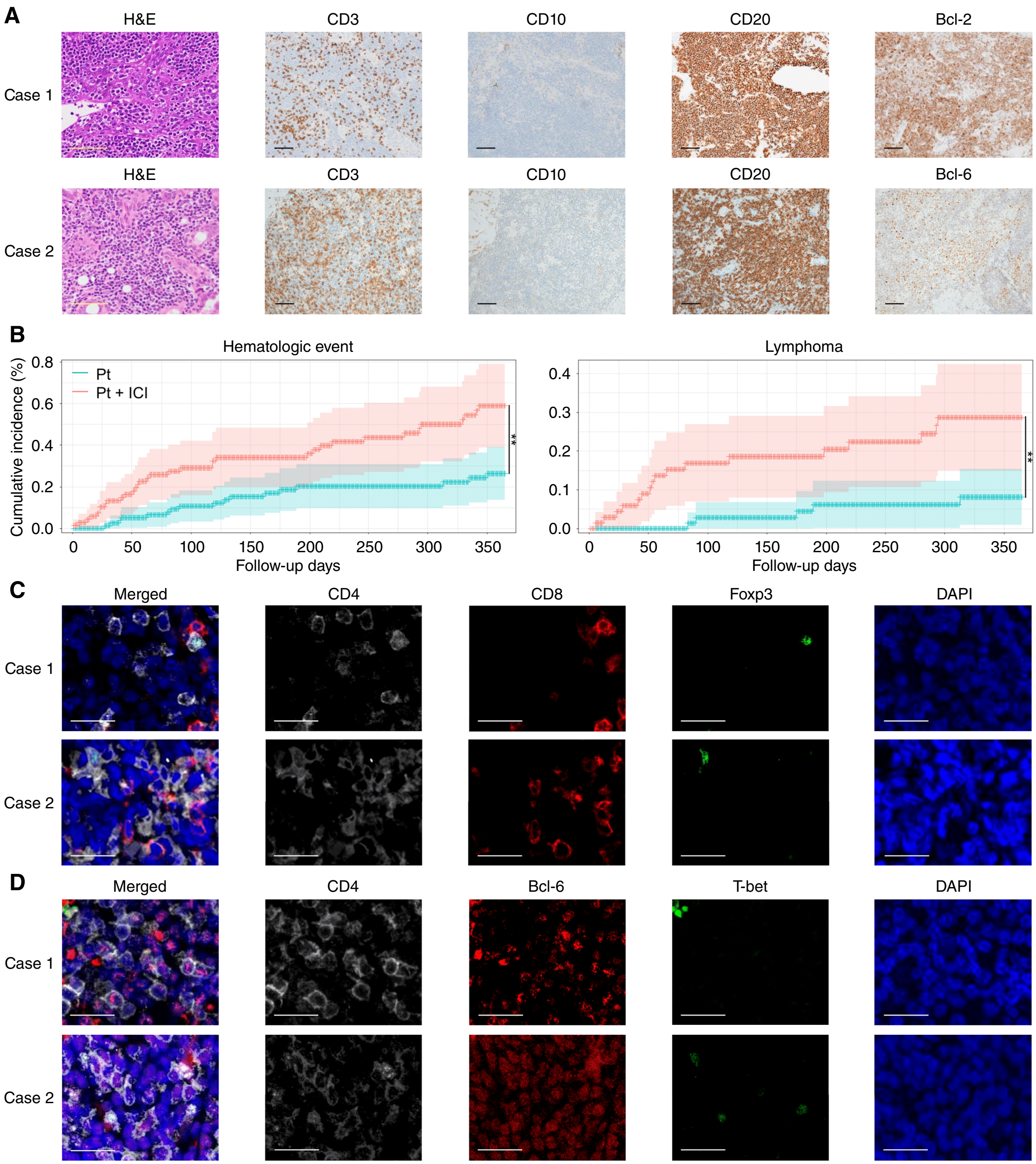

Figure 2.

Sample analyses of our identified B-cell lymphomas during PD-1 blockade therapies and the incidence of lymphomas from large-scale real-world data analyses. **A,** Pathologies of cases 1 (top) and 2 (bottom). H&E, CD3, CD10, CD20, and Bcl-2 or Bcl-6 staining for diagnosis are shown. Scale bar, 100 μm. **B,** Cumulative incidence of hematologic events (left) and lymphoma (right) with ICIs. The cumulative incidence of hematologic events, including lymphoma, leukemia, and multiple myeloma, in patients with lung cancer who received platinum doublets combined with ICIs (Pt + ICI) was compared with those who received platinum doublets without Pt. **C** and **D,** Multicolor IHC images of cases 1 (top) and 2 (bottom). CD4, CD8, FOXP3, Bcl-6, and T-bet were visualized by multicolor IHC using fluorophore-conjugated secondary antibodies. Representative staining results (**C**: CD4, CD8, and Foxp3; **D**: CD4, Bcl-6, and T-bet) are shown. Scale bar, 25 μm. Cumulative incidence was analyzed using the Kaplan–Meier method and compared among the groups using the log-rank test. **, $P < 0.01$.

However, 2.5 years after the initiation of nivolumab, she developed cervical erythema during nivolumab monotherapy, in which pathology showed primary cutaneous follicle center lymphoma, that is, invasion of the large-sized atypical lymphoid population in H&E staining with the IHC patterns of CD3^{-}, CD10^{-}, CD20^{+}, and BCL-6^{+} (**Fig. 2A**).

The incidence of lymphoma in patients with lung cancer can be related to the history of ICIs

These two cases prompted us to investigate the relationship between PD-1 blockade therapy and the incidence of hematologic malignancies. For this purpose, we first analyzed the MDV dataset. Between January 2010 and December 2021, 289,726 patients with lung cancer underwent therapy. The Pt + ICI group included patients who received initial prescriptions of ICIs and platinum-based anticancer agents [Pt: carboplatin (CBDCA) or cisplatin (CDDP)] between January 2017 and December 2021. As a control group, patients who received their initial prescription of platinum-based chemotherapy alone between January 2010 and December 2014 were included because ICIs were not approved during this period in Japan. In total, 17,129 and 10,055 patients were allocated to the Pt and Pt + ICI groups, respectively. Based on the exclusion criteria shown in Supplementary Fig. S1, 11,514 patients were excluded from the study. Ultimately, 8,661 patients in the Pt group and 7,009 in the Pt + ICI group were included for evaluation. The baseline characteristics of the patients are summarized in Supplementary Table S6. A retrospective analysis of clinical treatment records was conducted to compare the cumulative incidence of hematologic events, including lymphoma, leukemia, and multiple myeloma, between the Pt and Pt + ICI groups. The analysis revealed that the Pt + ICI group had a significantly higher cumulative incidence of hematologic events, particularly lymphoma, than the Pt group (**Fig. 2B**). We were unable to reliably distinguish B-cell lymphomas from T-cell lymphomas, owing to insufficient information on histologic subtypes in the MDV database. A competing risk refers to a scenario in which the prior occurrence of another competing event, such as death or radiotherapy, prevents an event of interest (target event). The failure to appropriately account for competing risks can introduce bias into the analysis. The Gray test is widely recognized for its effectiveness in comparing cumulative incidence rates while accounting for competing risks (35, 36). In this study, two competing risks—death and radiotherapy—were considered among the censoring criteria to analyze the occurrence of hematologic events. Even after accounting for competing risks, such as death and censoring due to radiotherapy, the cumulative incidence of hematologic events remained significantly higher in the Pt + ICI group than in the Pt group (Supplementary Fig. S5A; Supplementary Table S6). Additionally, the cumulative incidence of lymphoma remained significantly higher in the Pt + ICI group than in the Pt group after accounting for competing risks (death and radiotherapy; Supplementary Fig. S5B; Supplementary Table S6). In contrast, when stratified by leukemia or multiple myeloma alone, no significant difference in the cumulative incidence was observed between the two groups (Supplementary Fig. S6). To evaluate the robustness of our primary finding that ICI increases lymphoma risk, we conducted sensitivity analyses adjusting for potential unmeasured confounders, including age, sex, smoking history, and platinum agent type (cisplatin or carboplatin). Subgroup analysis demonstrated consistently elevated relative risks across all examined subgroups in the Pt + ICI group compared with the Pt group (Supplementary Table S7). We also confirmed a slight, but not dramatic, increase in both the crude and age-standardized incidence rates of lymphoma from 2010 to 2020 in Japan (Supplementary Fig. S7). Specifically, the age-standardized incidence rate of lymphoma increased approximately 1.5-fold over this period. Even after accounting for this secular increase in background incidence, the elevated lymphoma risk observed among ICI-treated patients remained substantial: The relative risk of approximately 3.9 derived from the MDV analysis of the cumulative incidence of lymphoma events with ICIs was conservatively attenuated to an adjusted relative risk of about 2.5, which is still markedly high. These results indicate a potential association between ICI and an increased risk of hematologic events, particularly lymphoma.

Therefore, we analyzed lymphoma cases associated with ICIs and their combination therapies using the WHO pharmacovigilance database from January 2017 to December 2023, the maximum duration available. Supplementary Figure S2 presents a flowchart outlining the patient selection process. The results of this analysis are summarized in Supplementary Table S8. Notably, 133 cases were identified, with pembrolizumab (58 cases) and nivolumab (53 cases) being the most commonly reported ICIs. Among the lymphoma subtypes, non-Hodgkin B-cell lymphoma accounted for 58 cases, followed by unclassified lymphomas (40 cases) and non-Hodgkin T-cell lymphoma (17 cases). Although Boudou-Rouquette and colleagues (37) reported the potential for lymphoma development following ICI therapy using the same database in 2019, our current analysis revealed that lymphoma cases continued to be reported after 2019 in association with ICI therapy. These findings highlight the rare but significant risk of hematologic adverse events caused by ICIs, particularly lymphomas.

T_{FH} cells highly infiltrated into the tumor microenvironment, which could be activated by PD-1 blockade therapies

Although PD-1 is expressed in various immune cell fractions, PD-1 blockade mainly promotes PD-1-expressing T-cell activation (38). Although PD-1 is reportedly expressed in B cells and can negatively regulate B-cell receptor signaling (39), PD-1 expression was limited in tumor-infiltrating B cells in our mouse experiments (Supplementary Fig. S4). In addition, PD-1 expression is also limited in B-cell lymphoma cells (40). Thus, we hypothesized that immune cells, particularly T cells, in the tumor microenvironment (TME) activated by PD-1 blockade may contribute to the development of malignant lymphoma. We assessed $CD4^-$-, $CD8^-$-, and FOXP3-expressing cell infiltration in FFPE samples from these two cases. Compared with other cells, a substantial infiltration of $CD4^+$ cells into the TME was observed and colocalized within the lymph follicles of malignant lymphoma, compared with $CD8^+$ cells or $FOXP3^+$ cells (**Fig. 2C**). We performed further multiplexed fluorescent IHC with T-Bet and Bcl-6 to distinguish between T_H1 and T_{FH} cells because these $CD4^+$ T-cell subsets reportedly express PD-1 (41). The results showed that tumor-infiltrating $CD4^+$ T cells were predominantly Bcl-6^+CD4^+ T_{FH} cells (**Fig. 2D**).

Therefore, we evaluated the effects of PD-1 blockade in T_{FH} cells. To induce T_{FH} cells, we used an established protocol as previously reported (34). Briefly, naïve $CD4^+$ T cells from mouse splenocytes were initially stimulated with gamma-irradiated APCs in the presence of anti-CD3 mAb and cultured in the medium supplemented with IL6 and IL21 for 4 days. PD-$1^+CXCR5^+FOXP3^-CD4^+$ T cells were used as T_{FH} cells for subsequent experiments because Bcl6 expression in this fraction was higher than in the other fraction (Supplementary Fig. S8A; refs. 42, 43). We also used a noncompetitive PD-1 antibody clone, RMP1-14, as previously reported (**Fig. 3A**; refs. 44, 45). The frequency of T_{FH} cells was increased by PD-1 blockade in the presence of gamma-irradiated APCs (**Fig. 3A**). ICOS, CD40L, T_{FH} cell activation molecules, and Ki67, a marker of proliferative capacity, showed similar trends (**Fig. 3B–D**). IL4 and IL21 production in T_{FH} cells also increased after the PD-1 blockade (**Fig. 3E** and **F**). Overall, T_{FH} cells highly infiltrated the TME of malignant lymphomas that developed during PD-1 blockade

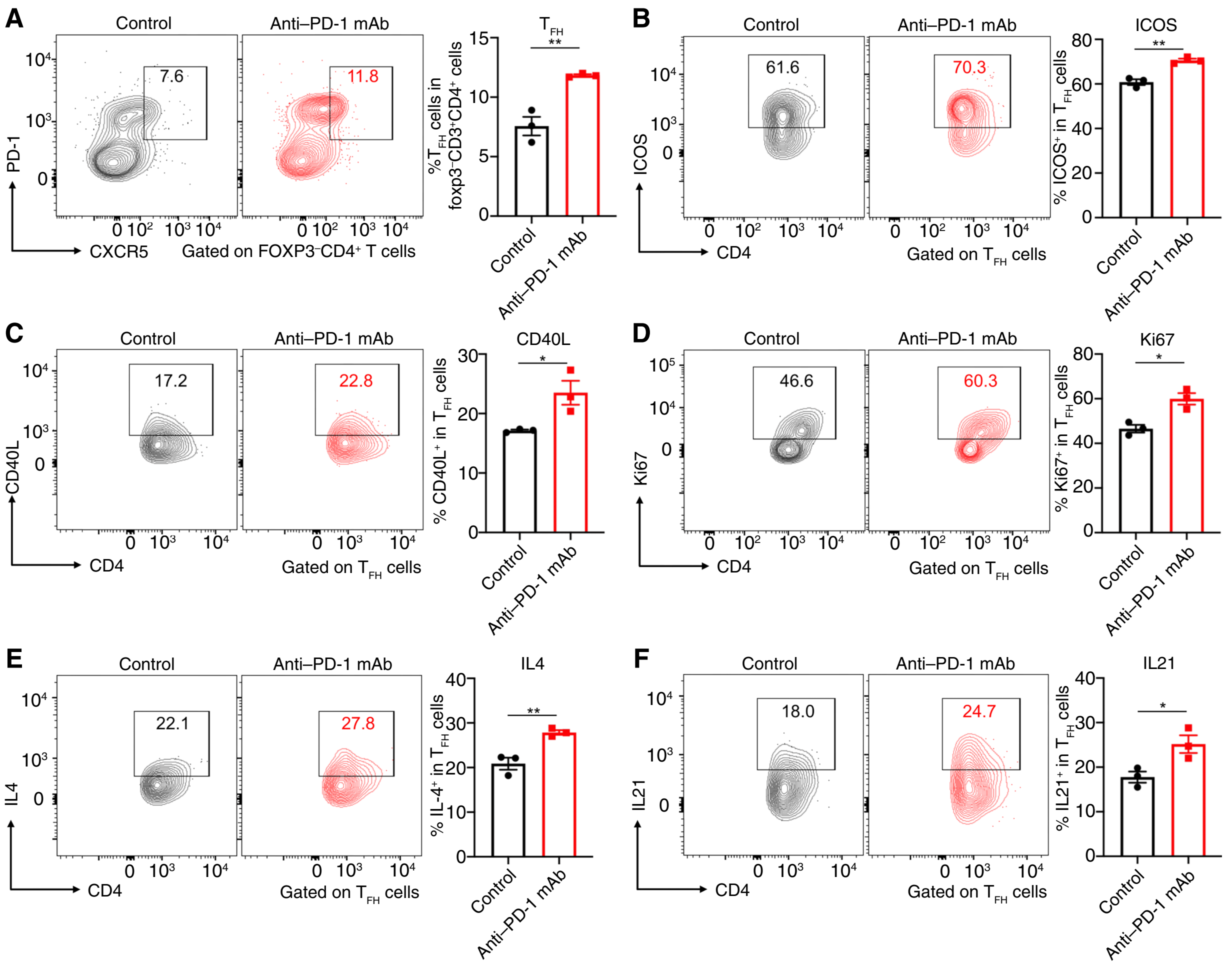

Figure 3.

CD4⁺ T_{FH} cell activation by PD-1 blockade *in vitro*. Purified mouse naïve CD4⁺ T cells were initially stimulated with gamma-irradiated APCs in the presence of anti-CD3 mAb and cultured in the medium supplemented with IL6 and IL21 for 4 days. Anti–PD-1 mAb was added on day 4. After 24 hours, the frequency of T_{FH} cells (**A**); ICOS (**B**), CD40L (**C**), and Ki67 (**D**) expression; and IL4 (**E**) and IL21 (**F**) production in T_{FH} cells were analyzed via flow cytometry. We gated T_{FH} cells as $PD\text{-}1^+CXCR5^+FOXP3^-CD4^+$ T cells. Representative flow cytometry staining (left) and summaries (right) are shown. *In vitro* experiments were performed in triplicate independently using three samples per group. Two-sided *t* tests were used for statistical analyses. *, $P < 0.05$; **, $P < 0.01$.

therapies, and PD-1 blockade activated T_{FH} cells, which could have an impact on malignant lymphoma cells.

IL4/IL4R or IL21/IL21R axis provided by T_{FH} cells can promote malignant lymphoma proliferation

As IL4 and IL21 produced by T_{FH} cells have been reported to be associated with the progression of malignant lymphoma (27–31), we assessed the impact of these factors on the proliferation of malignant lymphoma cells. After confirming the expression of the common γ chain (CD132), we retrovirally overexpressed the IL4 and IL21 receptors in the malignant lymphoma cell line E.G7 (E.G7/Il4r/Il21r; Supplementary Fig. S9A). *In vitro* experiments showed that the proliferation of E.G7/Il4r/Il21r, but not E.G7/Mock, was promoted in the presence of IL4 or IL21, which was abrogated by IL4 or IL21 blockade, respectively (**Fig. 4A** and **B**). When we evaluated the proliferation with CFSE, similar trends were observed (Supplementary Fig. S9B–S9E). We evaluated the downstream pathways of IL4 and IL21 using Western blotting. Consistently, E.G7/Il4r/Il21r cells treated with IL4 or IL21 had higher levels of pSTAT6 or pSTAT3, which were abrogated by IL4 or IL21 blockade, respectively (**Fig. 4C** and **D**). In contrast, the expression in E.G7/Mock cells was comparable with or without treatment (**Fig. 4C** and **D**).

We investigated the proliferation of E.G7/Il4r/Il21r under the condition of coculture with T_{FH} cells *in vitro*. CD40, which directly interacts with CD40L expressed in T_{FH} cells, was not expressed in E.G7 cells, suggesting that direct T_{FH}–tumor cell interactions play only a minor role in this model (Supplementary Fig. S9F). Thus, we used a transwell system during the coculture to specifically evaluate the effects of T_{FH} cell–derived cytokines. As expected, the proliferation of E.G7/Mock cells was comparable across all conditions, whereas the proliferation of E.G7/Il4r/Il21r cells was selectively promoted in the presence of T_{FH} cells induced as described above, but not in the presence of naïve $CD62L^+CD25^-CD4^+$ T cells (**Fig. 4E**). In addition, this enhanced proliferation was specifically inhibited by IL4/IL21 blockade (**Fig. 4F**). These results indicate that IL4 and IL21 produced by T_{FH} cells can promote the proliferation of

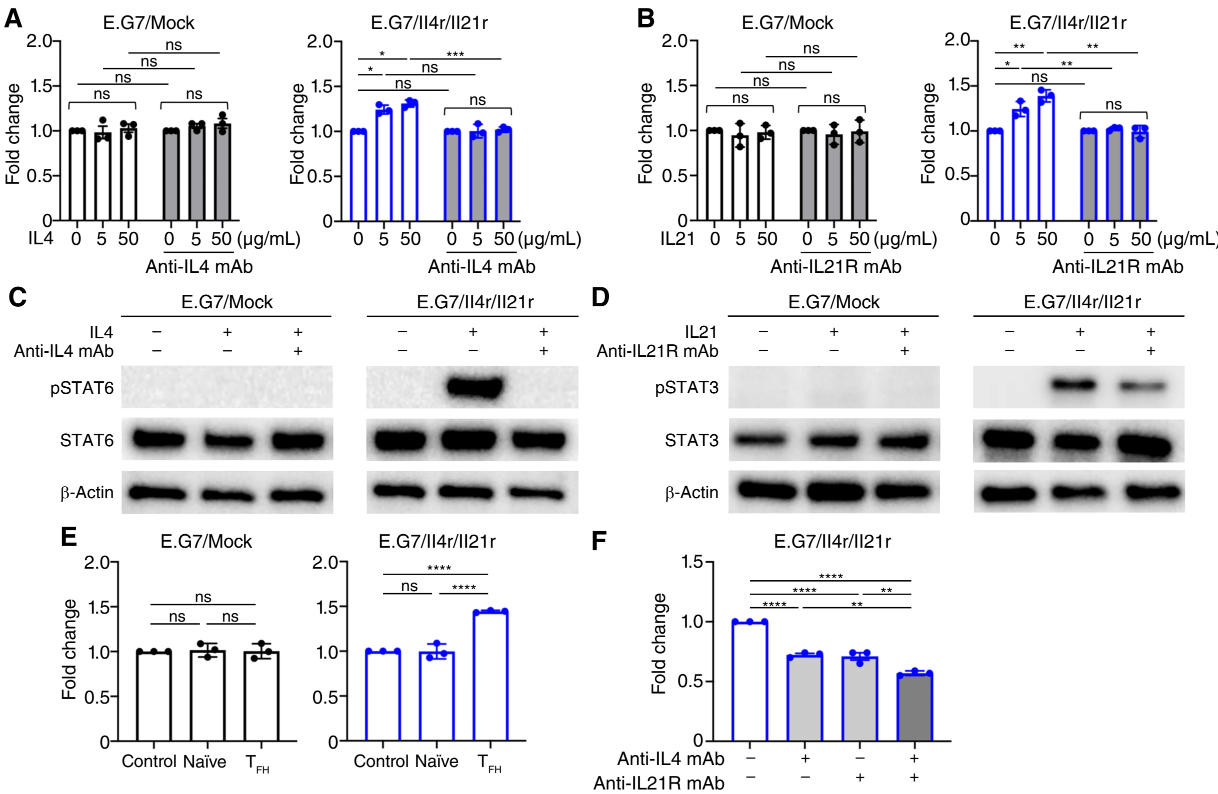

Figure 4.

Influence of IL4 and IL21 produced by $CD4^+$ T_{FH} cells on lymphoma cells expressing the corresponding receptors. **A,** Cellular proliferation of E.G7/Mock and E.G7/Il4r/Il21r cells in the presence of IL4. Cells were treated with IL4 at the indicated concentrations with or without anti-IL4 mAb. After 48 hours, the proliferation was assessed using a CCK-8 assay, and summaries (left, E.G7/Mock; right, E.G7/Il4r/Il21r) are shown. **B,** Cellular proliferation of E.G7/Mock and E.G7/Il4r/Il21r cells in the presence of IL21. Cells were treated with IL21 at the indicated concentrations, with or without anti-IL21R mAb. After 48 hours, the proliferation was assessed using a CCK-8 assay, and summaries (left, E.G7/Mock; right, E.G7/Il4r/Il21r) are shown. **C** and **D,** Western blotting of the STAT6 (**C**) and STAT3 (**D**) signaling pathways. Following treatment with IL4 (**C**) or IL21 (**D**) for 30 minutes, cells were collected, and the whole-cell lysates were analyzed. **E,** Cellular proliferation of E.G7/Mock and E.G7/Il4r/Il21r cells cocultured with naïve $CD4^+$ T cells or T_{FH} cells. $CD62L^+CD25^-CD4^+$ T cells (naïve $CD4^+$ T cells) were sorted from mouse splenocytes, and $PD\text{-}1^+CXCR5^+CD25^-CD4^+$ T cells (T_{FH} cells) were sorted from mouse splenocytes cultured under the T_{FH} cell induction condition, which were subsequently cocultured with E.G7 cells using a transwell plate. After 48 hours, the proliferation was assessed using a CCK-8 assay, and summaries (left, E.G7/Mock; right, E.G7/Il4r/Il21r) are shown. **F,** Cellular proliferation of E.G7/Il4r/Il21r cells cocultured with T_{FH} cells in the presence of anti-IL4 and/or IL21R mAbs. The proliferation was evaluated as described in **E** with or without anti-IL4 and/or IL21R mAbs, and a summary is shown. *In vitro* experiments were performed in triplicate independently using three samples per group. One-way ANOVA with Bonferroni correction was used in **A**, **B**, **E**, and **F** for statistical analyses. *, $P < 0.05$; **, $P < 0.01$; ***, $P < 0.001$; ****, $P < 0.0001$; ns, not significant.

malignant lymphoma cells when they express their corresponding receptors.

PD-1 blockade promotes malignant lymphoma proliferation through the activation of T_{FH} cells *in vivo*

To clarify whether T_{FH} cells activated by the PD-1 blockade lead to the progression of malignant lymphoma, we conducted *in vivo* experiments. The control E.G7/Mock tumors responded to PD-1 blockade in wild-type mice, whereas E.G7/Il4r/Il21r tumors not only failed to respond but also exhibited accelerated growth upon PD-1 blockade (**Fig. 5A**). When we used another lymphoma A20 cell line, similar trends were observed in A20/Il4r/Il21r tumors (Supplementary Figs. S9G and S10A). In *Cd4*^{cre}*Bcl6*$^{flox/flox}$ mice lacking T_{FH} cells (Supplementary Fig. S10B), the E.G7/Il4r/Il21r tumors were not exacerbated by PD-1 blockade but were comparable with the control tumors (**Fig. 5B**). By comparing the untreated groups for both E.G7/Mock and E.G7/Il4r/Il21r in wild-type and *Cd4*^{cre}*Bcl6*$^{flox/flox}$ mice, tumor growth was comparable between wild-type and *Cd4*^{cre}*Bcl6*$^{flox/flox}$ mice, indicating that T_{FH} cells could promote tumor progression, particularly during PD-1 blockade in the E.G7 model. Although B cells in TILs showed high CXCR5 expression, they were identified as $CD3^-B220^+$ cells with minimal PD-1 expression. In contrast, T_{FH} cells showed relatively low CXCR5 but clearly high PD-1 expression and were also defined as $PD\text{-}1^+CXCR5^+FOXP3^-CD4^+CD3^+$ T cells in TILs (Supplementary Figs. S3 and S4; refs. 42, 43). Accordingly, Bcl6 was coexpressed in this fraction, and the expression was higher than in the other fraction from dLNs (Supplementary Fig. S8B; refs. 42, 43). PD-1 blockade increased T_{FH} cells, elevated ICOS and CD40L expression, and increased IL4 and IL21 production in TILs (**Fig. 5C–G**). Because T_{FH}/B-cell interactions mainly take place in the dLNs, we additionally analyzed the dLNs using the same mouse models. ICOS, CD40L, IL4, and IL21 expression were significantly higher in T_{FH} cells than in non-T_{FH}/T_{reg} $CD4^+$ T cells within dLNs (Supplementary Fig. S10C–S10F). Following PD-1 blockade, both the

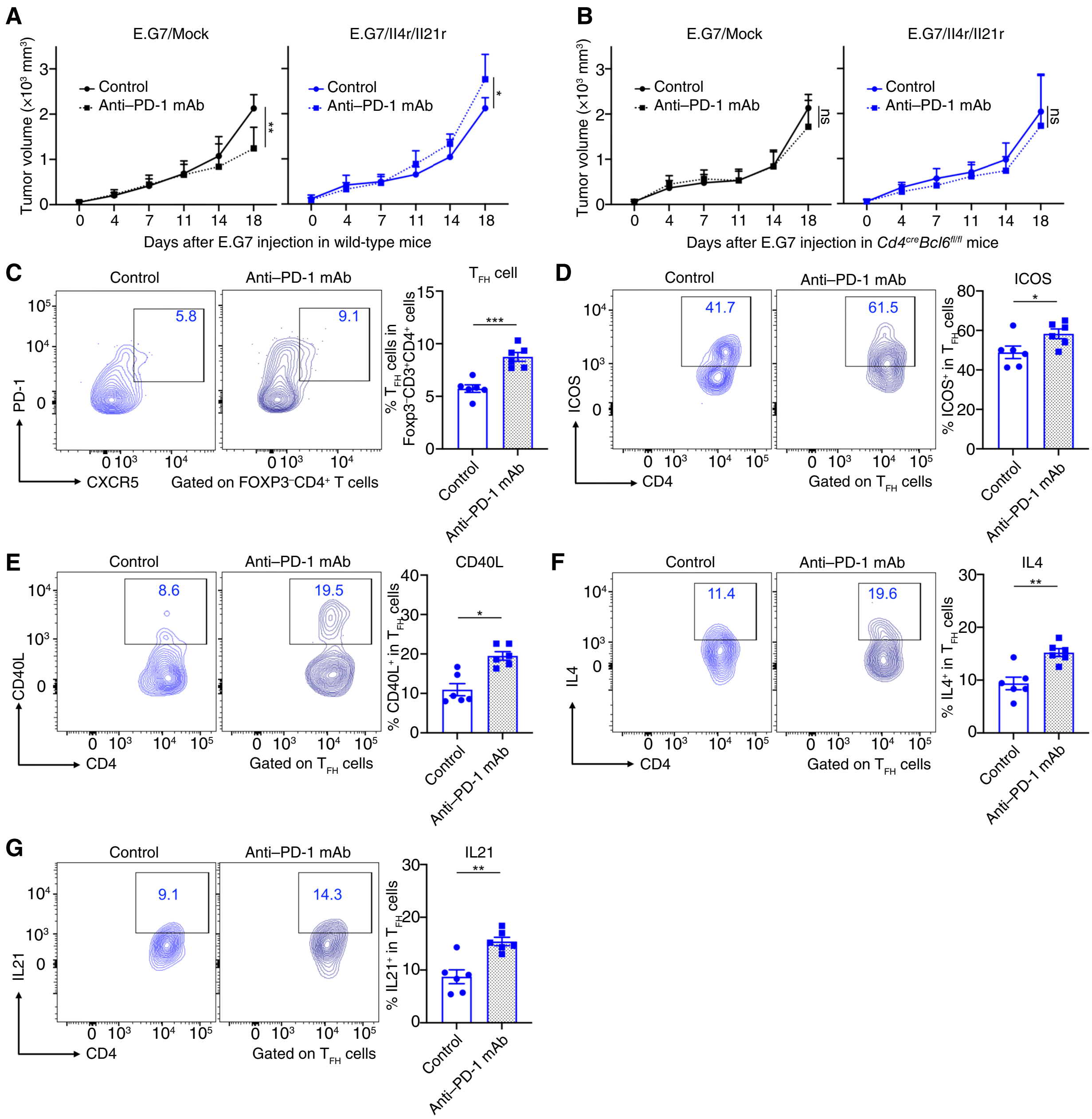

Figure 5.

In vivo efficacy of PD-1 blockade against IL4R/IL21R-expressing tumors. **A** and **B,** Tumor growth of E.G7 in wild-type mice (**A**) and *Cd4*^{cre}*Bcl6*$^{fl/fl}$ (**B**) mice. E.G7 cells were injected subcutaneously, and the tumor volume was monitored twice a week. The means of the long and short tumor diameters were used to generate tumor growth curves. The mice were grouped on day 7, and the anti–PD-1 mAb or control mAb was administered intraperitoneally three times every 3 days. Tumor growth curves (left, E.G7/Mock; right, E.G7/Il4r/Il21r) are shown. **C–G,** TIL analyses in wild-type mice. *In vivo* experiments were performed as described in **A**. Tumors were harvested 7 days after treatment initiation for TIL analysis. The frequency of CD4$^+$ T$_{FH}$ cells in TILs (**C**), ICOS (**D**), and CD40L (**E**) expression and IL4 (**F**) and IL21 (**G**) production in tumor-infiltrating T$_{FH}$ cells were analyzed via flow cytometry. For intracellular cytokine assays, cells were stimulated with anti-CD3 and CD28 mAbs. We gated T$_{FH}$ cells as PD-1$^+$CXCR5$^+$FOXP3$^-$CD4$^+$ T cells. Representative flow cytometry staining (left) and summaries (right) are shown. *In vivo* experiments were performed at least twice. Two-way ANOVA was used in **A** and **B**, and two-sided *t* tests were used in **C–G** for statistical analyses. *, $P < 0.05$; **, $P < 0.01$; ***, $P < 0.001$; ns, not significant.

frequency of T$_{FH}$ cells and their expression of ICOS, CD40L, IL4, and IL21 further increased, whereas the expression of these molecules in non-T$_{FH}$/T$_{reg}$ CD4$^+$ T cells remained comparable (Supplementary Fig. S10C–S10G). In addition, the frequencies of B cells and GL7$^+$FAS$^+$ GC B cells also increased after PD-1 blockade (Supplementary Fig. S10H and S10I). In contrast, PD-1 blockade had comparable effects on T$_{reg}$ cells in TILs (Supplementary Fig. S10J and S10K).

The CD40L/CD40 axis provided by T_{FH} cells can also promote malignant lymphoma proliferation

In addition to IL4 and IL21, CD40L expression in T_{FH} cells has been reported to be related to the progression of malignant lymphoma, and our TIL analyses showed that CD40L expression in T_{FH} cells was elevated by PD-1 blockade (31). Thus, we retrovirally overexpressed CD40 in E.G7 cells (E.G7/Cd40), but sCD40L did not promote proliferation (Supplementary Fig. S9F and S9H). Considering the differences in the downstream pathways, we used the A20 cell line. Because this cell line expressed CD40, we created a CD40 knockout A20 cell line using the CRISPR/Cas9 system (A20/Cd40KO; Supplementary Fig. S9I). Although proliferation was comparable between control A20 and A20/Cd40KO cells, sCD40L promoted proliferation in control A20 cells, but not in A20/Cd40KO cells (**Fig. 6A**). This promoted proliferation was inhibited by CD40 blockade (**Fig. 6A**). We evaluated the downstream pathways of CD40 using Western blotting, which showed that control A20 cells treated with sCD40L had a higher level of pAKT, which was reversed by CD40 blockade (**Fig. 6B**). In contrast, the levels in the A20/Cd40KO cells were comparable (**Fig. 6B**). Accordingly, A20 tumors grew rapidly with no response to PD-1 blockade compared with A20/Cd40KO tumors, which showed slow growth with response (**Fig. 6C**). These findings indicate that in the absence of CD40 signaling, the dominant effect of PD-1 blockade is to enhance antitumor immunity, underscoring the importance of CD40 signaling pathways in the A20 tumor model, which seems to be different from those in the E.G7 tumor model. In contrast, as shown in Supplementary Fig. S10A, A20/Il4r/Il21r tumors exhibited accelerated growth upon PD-1 blockade, suggesting that strong T_{FH} cell–derived cytokine signaling, in addition to CD40 input, can override the antitumor immune response when the corresponding receptors are abundantly expressed on lymphoma cells.

PD-1 blockade can promote malignant lymphoma progression via T_{FH} cells

Finally, we stained IL4R, IL21R, and CD40 in the two patients who developed malignant lymphoma during PD-1 blockade therapies. Consistent with this, we observed their expression in lymphoma cells (Supplementary Fig. S11). Overall, tumor-infiltrating T_{FH} cells activated by the PD-1 blockade promote malignant lymphoma progression via the IL4/IL4R, IL21/IL21R, and CD40L/CD40 axes when the lymphoma cells express the corresponding receptors.

To compare other lymphomas in the absence of ICI treatment, we examined 10 conventional B-cell lymphomas, including FL and DLBCL (Supplementary Fig. S12). We found that three of the five FLs and two of the five DLBCLs exhibited high T_{FH} cell infiltration (Supplementary Figs. S13 and S14; Supplementary Table S1). Notably, both DLBCLs with high infiltration were of the GC B cell–like subtype (GCB-DLBCL). Furthermore, IL4R, IL21R, and CD40 expressions were high in all FL cases but heterogeneous in DLBCL (Supplementary Fig. S15; Supplementary Table S1). These suggest that such lymphoma subtypes also have the potential for development during ICI treatment.

Discussion

ICIs have been considered viable and attractive treatment options for patients with various types of cancer, including lung cancer, and a huge number of patients have received ICIs worldwide for years (2–5). Thus, the novel and unexpected complications of long-term

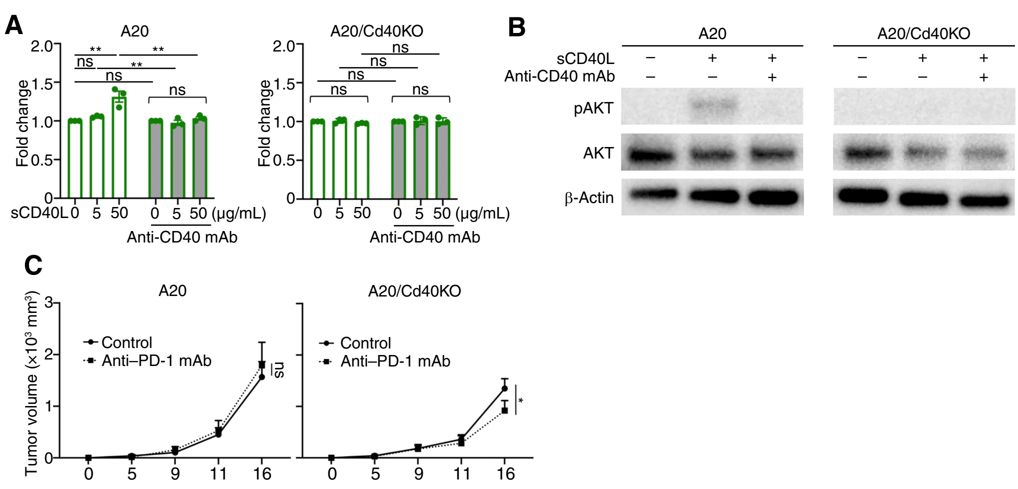

Figure 6.

Influence of CD40 signaling in CD40-expressing lymphoma cells. **A,** Proliferation of A20 and A20/Cd40KO cells in the presence of sCD40L. Cells were treated with sCD40L at the indicated concentrations, with or without anti-CD40 mAb. After 48 hours, the proliferation was assessed using a CCK-8 assay, and summaries (left, A20; right, A20/Cd40KO) are shown. **B,** Western blotting for the PI3K signaling pathways. Following treatment with sCD40L for 30 minutes, cells were collected and the whole-cell lysates were analyzed. **C,** Tumor growth of A20 in wild-type mice. A20 cells were injected subcutaneously, and the tumor volume was monitored twice a week. The means of the long and short tumor diameters were used to generate tumor growth curves. The mice were grouped on day 7, and the anti–PD-1 mAb or control mAb was administered intraperitoneally three times every 3 days. Tumor growth curves (left, A20; right, A20/Cd40KO) are shown. *In vitro* experiments were performed in triplicate independently using three samples per group, and *in vivo* experiments were performed at least twice. One-way ANOVA with Bonferroni correction was used for statistical analyses **A** and **B**. Two-way ANOVA was used in **C**. *, $P < 0.05$; **, $P < 0.01$; ns, not significant.

use are becoming more apparent. Among these complications, we found a higher incidence of hematologic malignancies, especially malignant lymphoma, in patients with lung cancer treated with PD-1 blockade therapy than in those without, based on large-scale real-world data analyses. We identified two cases of B-cell lymphoma after PD-1 blockade therapy, in which the histology was MALT lymphoma or primary cutaneous follicle center lymphoma with a large amount of T_{FH} cell infiltration. In our *in vitro* and *in vivo* experiments, PD-1 blockade activated T_{FH} cells, promoting malignant cell proliferation with the corresponding receptors via cytokine production and CD40L expression. Although previous reports have shown the incidence of hematologic malignancies after ICI treatment (37, 46), our study provides mechanistic insight into how malignant lymphoma may develop during ICI treatment.

The T_{FH} cells provide essential assistance to B cells for an effective antibody-mediated immune response. In addition to their crucial functions in infection and vaccination, their involvement in cancer has begun to emerge (26). T_{FH} cell infiltration in various solid tumors of nonlymphocytic origin is associated with better prognosis and is involved in tertiary lymphoid structures (TLS; refs. 23–26). Several groups, including ours, have demonstrated that T_{FH} cell infiltration with TLS enhances antitumor immunity and ICI efficacy by promoting $CD8^+$ T cells in solid tumors (11, 21–23). Consistent with this, we also observed that T_{FH} cell knockout impaired ICI efficacy, as shown in **Fig. 5**. In particular, IL4 and IL21 produced by T_{FH} cells activated by PD-1 blockade strongly support the $CD8^+$ T cells that attack tumor cells (21–23). In contrast to solid tumors, T_{FH} cells in B-cell malignancies are often associated with unfavorable outcomes (26–31). This could be explained by the presence of several factors in T_{FH} cells, including IL4, IL21, and CD40L (27–31). These factors originally promote B-cell survival and proliferation (13, 26). Thus, when malignant B cells express their corresponding receptors, T_{FH} cells can promote malignant cell survival and proliferation (14–16, 26). In addition, our experiments have shown that PD-1 blockade activates tumor-infiltrating T_{FH} cells along with high IL4 and IL21 production and high CD40L expression because T_{FH} cells highly express PD-1. As a result, in malignant cells harboring the corresponding receptors, tumor cell survival and proliferation are promoted in a manner that may surpass the elimination mechanisms mediated by $CD8^+$ T cells with the help of T_{FH} cells. We also acknowledge that in our *in vitro* system, the frequency of induced T_{FH} cells was relatively modest compared with some published protocols, likely reflecting the differences in stimulation conditions (APC-priming or antigen-specific stimulation; ref. 34). However, the comparison between T_{FH} cell–deficient and control mice *in vivo* supports the notion that even a numerically small T_{FH} cell fraction can exert biologically meaningful effects on lymphoma progression. Furthermore, although PD-1 expression was limited in tumor-infiltrating B cells in our mouse experiments, PD-1 is reportedly expressed in B cells and can negatively regulate B-cell receptor signaling (39), suggesting possible B cell–intrinsic effects of PD-1 blockade and potential B-cell feedback on T_{FH} cell activation. We found two patients who developed B-cell lymphoma after PD-1 blockade therapy, and these lymphomas had the corresponding receptors with a huge amount of T_{FH} cell infiltration. This is consistent with previous studies showing unfavorable outcomes in B-cell malignancies (27–31). In addition, a significant proportion of lymphomas in the absence of ICI treatment, particularly GC-derived lymphomas such as FL and GCB-DLBCL, also exhibited substantial T_{FH} cell infiltration and expressed the corresponding receptors, consistent with previous reports (47, 48). These findings suggest that such lymphomas also have the potential to develop during ICI treatment. Overall, T_{FH} cells are double-edged swords. In other words, they can help $CD8^+$ T cells that attack tumor cells but can promote the survival and proliferation of B-cell malignant cells harboring the corresponding receptors (IL4/IL21 receptors and CD40).

Our A20 tumor models further illustrate this context-dependent balance. In control A20 tumors, which express CD40 but do not overexpress IL4R/IL21R, PD-1 blockade did not result in a measurable net change in tumor growth, consistent with a scenario in which T_{FH} cell–derived CD40 input and enhanced antitumor immunity approximately counterbalance each other. In A20/Cd40KO tumors, CD40-mediated input is lost, and PD-1 blockade predominantly amplifies antitumor immunity, leading to reduced tumor growth. Conversely, in A20/Il4r/Il21r tumors, PD-1 blockade enhanced tumor growth, indicating that strong T_{FH} cell–derived IL4/IL21 cytokine signaling, in addition to CD40-mediated input, can tip the balance toward lymphoma promotion despite concomitant activation of antitumor immunity. Together, these findings support a unified model in which PD-1 blockade–induced T_{FH} cell activation exerts opposing effects, with the net outcome depending critically on the receptor profile of the malignant B cells and the balance between T_{FH} cell–derived trophic signals and antitumor immunity.

Several studies have reported a reduced risk of solid tumors in patients treated with ICIs, suggesting that ICIs also inhibit micro solid tumors (49–52). However, unlike the present study, these studies did not focus on hematologic malignancies. In contrast, other previous studies have shown the incidence of hematologic malignancies after ICI treatment (37, 46), and the present study showed a higher incidence and one of the detailed mechanisms. In addition, PD-1 blockade therapies have been used for hematologic malignancies, showing disappointing results except for Hodgkin lymphoma (40, 53–57). In particular, high frequencies of progressive disease (PD) have been observed in clinical trials, which may be partially explained by our findings (55–57). In other words, T_{FH} cells activated by PD-1 blockade could promote the survival and proliferation of malignant cells harboring the corresponding receptors (IL4, IL21, and CD40) in such patients. Thus, these receptors could be used as PD markers for PD-1 blockade therapy in hematologic malignancies. However, considering their roles as double-edged swords, they can also help $CD8^+$ T cells that attack malignant cells in responders.

MALT and primary cutaneous follicle center lymphomas are classified as indolent B-cell lymphomas, and malignant cell proliferation is generally slow (58). Given the supportive roles of T_{FH} cells, the slow proliferation of malignant cells, and limited PD-1 expression in B-cell lymphoma cells, T_{FH} cells activated by PD-1 blockade may be related to the proliferation of B-cell malignancies rather than direct carcinogenesis. Although we did not find other types of lymphoma, such as DLBCL, during ICI treatment, FL and GCB-DLBCL could also have the potential to develop during ICI treatment because they have abundant T_{FH} cell infiltration, as observed by us (47, 48).

ICIs reportedly contribute to long-term survival in patients with lung cancer (59), which could be related to the higher incidence of hematologic malignancies in patients who received ICIs in our cohort. To avoid such biases, we analyzed only 1-year clinical courses after the initiation of first-line chemotherapies with or without ICIs, while also accounting for death as a competing risk, showing a higher incidence (~3.9). However, analyzing patients over a longer period might reveal an even higher incidence, as seen in cases we identified in which lymphomas were diagnosed more than 2 years after the initiation of PD-1 blockade therapy. Otherwise, we could not directly compare the frequencies during the same period because most patients used ICIs after approval, and the small subset of patients who did not receive ICIs did so due to specific clinical circumstances. Although approved cytotoxic chemotherapies for lung cancer remained almost unchanged during this period, our analyses could have included some biases. At the population level, national cancer registry data indicate that the incidence of lymphoma in Japan has increased modestly over the study period (~1.5), which could potentially introduce bias. Importantly, even after accounting for this temporal increase in background incidence, the occurrence of lymphoma in the Pt + ICI group remained substantially higher (~2.6), suggesting that the observed association cannot be explained solely by temporal trends in lymphoma epidemiology. Moreover, our study provides complementary mechanistic evidence both *in vitro* and *in vivo*, which helps mitigate concerns about potential bias. A further limitation of our clinical database analysis is that we were unable to reliably distinguish B-cell lymphomas from T-cell lymphomas in the MDV database, owing to insufficient information on histologic subtypes. In the WHO pharmacovigilance database, however, B-cell lymphomas accounted for many of the events. In addition, both our pathologically confirmed cases were B-cell lymphomas with abundant T_{FH} cell infiltration. Thus, we focused our experimental work on the T_{FH} B–cell axis. In contrast, PD-1 also functions as a haplo-insufficient tumor suppressor in T-cell lymphomas (60, 61), and our data do not exclude an increased risk of T-cell lymphomas under PD-1 blockade. Overall, larger prospective studies are required to accurately elucidate their frequency and clinicopathologic features.

In summary, we found a higher incidence of hematologic malignancies, especially B-cell malignancies, in patients with lung cancer treated with PD-1 blockade therapy than in those without, based on large-scale data analyses. Our identified B-cell lymphoma after PD-1 blockade therapies had large amounts of T_{FH} cell infiltration, and PD-1 blockade could activate T_{FH} cells, promoting lymphoma proliferation via the IL4/IL4R, IL21/IL21R, and CD40L/CD40 axes *in vitro* and *in vivo*. These findings provide novel insights into potential B-cell malignancy complications in clinical settings in which ICIs are used, to which attention should be paid.

Data Availability

The MDV and VigiBase databases are not publicly available because access is restricted under data-use agreements, and the deidentified patient-level data they contain are subject to patient privacy protections and contractual restrictions. All raw data supporting the findings of this study, including imaging data and experimental results from *in vitro* and animal studies, are available from the corresponding author upon reasonable request.

Authors' Disclosures

D. Ennishi reports grants and personal fees from Nippon Shinyaku Pharmaceutical Co. Ltd., Chugai Pharmaceutical Co. Ltd., and Eisai Co. Ltd.; grants from Insight Co. Ltd.; and personal fees from AbbVie GK, Bristol Myers Squibb, Ono Pharmaceutical Co. Ltd., Genmab A/S, Janssen Pharmaceutical, Novartis Pharma K.K., Otsuka Pharmaceutical Co. Ltd., Incyte Biosciences Japan GK, BeOne Medicines Ltd., Kyowa Kirin Pharmaceutical Co. Ltd., and AstraZeneca K.K. outside the submitted work. K. Ohashi reports grants from the Japan Society for the Promotion of Science during the conduct of the study, as well as grants and personal fees from Boehringer Ingelheim and Chugai Pharmaceutical and personal fees from Amgen, Pfizer, Eli Lilly, AstraZeneca, MSD, Novartis, Ono Pharmaceutical, and Bristol Myers Squibb outside the submitted work. S. Morizane reports grants from Sun Pharma, grants and personal fees from Maruho, and personal fees from Eli Lilly, UCB, AbbVie, Pfizer, Torii Pharmaceutical, Sanofi, and Boehringer Ingelheim outside the submitted work. Y. Maeda reports grants from Otsuka Pharmaceutical, Takeda Pharmaceutical, Kyowa Kirin, Nippon Shinyaku, and Chugai Pharma, as well as personal fees from Kyowa Kirin, Pfizer, Novartis Pharmaceutical, and Takeda Pharmaceutical outside the submitted work. I. Okamoto reports grants from AstraZeneca, Chugai Pharmaceutical, MSD, Daiichi Sankyo, Bristol Myers Squibb, Boehringer Ingelheim, Amgen, Taiho Pharmaceutical, and GSK outside the submitted work. J. Nagasaki reports grants from the Japan Society for the Promotion of Science, the Uehara Memorial Foundation, the Kowa Life Science Foundation, the Chugai Foundation for Innovative Drug Discovery Science, the Naito Foundation, the Yasuda Medical Foundation, the Nippon Shinyaku Public Research Grant, Kato Memorial Bioscience Foundation, the Japanese Society of Hematology Research Grant, and the Ichiro Kanehara Foundation during the conduct of the study. Y. Togashi reports grants from the Japan Society for the Promotion of Science, Japan Agency for Medical Research and Development, Japan Science and Technology Agency, National Cancer Center Research and Development Fund, Wescoe Foundation, Project Mirai Cancer Research Grants, Japan Research Foundation for Clinical Pharmacology, and Naito Foundation during the conduct of the study, as well as personal fees from Ono Pharmaceutical, Bristol Myers Squibb, and Chugai Pharmaceutical; grants and personal fees from AstraZeneca; personal fees from Eisai and MSD; and grants from Daiichi Sankyo, KORTUC, Janssen, Takeda, and Taiho outside the submitted work. No disclosures were reported by the other authors.

Authors' Contributions

T. Ninomiya: Data curation, formal analysis, writing–original draft. **C. Fang:** Data curation, formal analysis. **H. Hamano:** Data curation, formal analysis, writing–original draft. **T. Morinaga:** Data curation, formal analysis. **W. Zhou:** Data curation, formal analysis. **T. Koyama:** Data curation. **S. Miki:** Data curation. **L. Zhu:** Data curation. **Y. Naoi:** Resources. **D. Ennishi:** Resources. **T. Katsuta:** Resources. **K. Ohashi:** Resources. **S. Morizane:** Resources. **T. Ohki-Ikeda:** Resources. **T. Nishi:** Resources. **Y. Ueda:** Resources. **T. Ishino:** Resources. **Y. Maeda:** Supervision. **I. Okamoto:** Supervision. **Y. Zamami:** Supervision. **J. Nagasaki:** Conceptualization, data curation, formal analysis, writing–original draft, project administration. **Y. Togashi:** Conceptualization, data curation, formal analysis, writing–original draft, project administration.

Acknowledgments

We thank M. Iwado, Y. Nishimori, R. Inukai, M. Konishi, and A. Ozasa, Department of Animal Resources, Advanced Science Research Center, Okayama University, and Central Research Laboratory, Okayama University Medical School, for their technical assistance. We would like to thank Editage (www.editage.com) and ChatGPT (chat.openai.com) for English language editing. This research was supported by grants from the Japan Society for the Promotion of Science [JP21H05051 (Y. Togashi), JP22K20824 (J. Nagasaki), JP23K14594 (J. Nagasaki), JP25K19576 (J. Nagasaki), JP23KK0149 (J. Nagasaki and Y. Togashi), and JP24K02459 (K. Ohashi and Y. Togashi)]; the Japan Agency for Medical Research and Development [CREST, no. JP22gm1810002 (Y. Togashi)]; Japan Science and Technology Agency [JPMJFR2049 (Y. Togashi)]; the National Cancer Center Research and Development Fund [no. 2023-A-05 (Y. Togashi)]; the Wescoe Foundation (Y. Togashi); the Uehara Memorial Foundation (J. Nagasaki); the Project Mirai Cancer Research Grants (Y. Togashi); the Kowa Life Science Foundation (J. Nagasaki); the Japan Research Foundation for Clinical Pharmacology (Y. Togashi); the Chugai Foundation for Innovative Drug Discovery Science (J. Nagasaki); the Naito Foundation (J. Nagasaki and Y. Togashi); the Yasuda Medical Foundation (J. Nagasaki); the Nippon Shinyaku Public Research Grant (J. Nagasaki); the Kato Memorial Bioscience Foundation (J. Nagasaki); the Japanese Society of Hematology Research Grant (J. Nagasaki); and the Ichiro Kanehara Foundation (J. Nagasaki).

Note

Supplementary data for this article are available at Clinical Cancer Research Online (http://clincancerres.aacrjournals.org/).

Received September 11, 2025; revised January 18, 2026; accepted April 10, 2026; posted first May 19, 2026.

References

1. Global Burden of Disease 2019 Cancer Collaboration; Kocarnik JM, Compton K, Dean FE, Fu W, Gaw BL, et al. Cancer incidence, mortality, years of life lost, years lived with disability, and disability-adjusted life years for 29 cancer groups from 2010 to 2019: a systematic analysis for the Global Burden of Disease Study 2019. JAMA Oncol 2022;8:420–44.
2. Hellmann MD, Paz-Ares L, Bernabe Caro R, Zurawski B, Kim SW, Carcereny Costa E, et al. Nivolumab plus ipilimumab in advanced non-small-cell lung cancer. N Engl J Med 2019;381:2020–31.
3. Socinski MA, Jotte RM, Cappuzzo F, Orlandi F, Stroyakovskiy D, Nogami N, et al. Atezolizumab for first-line treatment of metastatic nonsquamous NSCLC. N Engl J Med 2018;378:2288–301.
4. Hodi FS, O'Day SJ, McDermott DF, Weber RW, Sosman JA, Haanen JB, et al. Improved survival with ipilimumab in patients with metastatic melanoma. N Engl J Med 2010;363:711–23.
5. Motzer RJ, Escudier B, McDermott DF, George S, Hammers HJ, Srinivas S, et al. Nivolumab versus everolimus in advanced renal-cell carcinoma. N Engl J Med 2015;373:1803–13.
6. Zou W, Wolchok JD, Chen L. PD-L1 (B7-H1) and PD-1 pathway blockade for cancer therapy: mechanisms, response biomarkers, and combinations. Sci Transl Med 2016;8:328rv4.
7. Nagasaki J, Ishino T, Togashi Y. Mechanisms of resistance to immune checkpoint inhibitors. Cancer Sci 2022;113:3303–12.
8. van der Leun AM, Thommen DS, Schumacher TN. $CD8^+$ T cell states in human cancer: insights from single-cell analysis. Nat Rev Cancer 2020;20: 218–32.
9. Nagasaki J, Inozume T, Sax N, Ariyasu R, Ishikawa M, Yamashita K, et al. PD-1 blockade therapy promotes infiltration of tumor-attacking exhausted T cell clonotypes. Cell Rep 2022;38:110331.
10. Miggelbrink AM, Jackson JD, Lorrey SJ, Srinivasan ES, Waibl-Polania J, Wilkinson DS, et al. CD4 T-cell exhaustion: does it exist and what are its roles in cancer? Clin Cancer Res 2021;27:5742–52.
11. Zhou W, Kawashima S, Ishino T, Kawase K, Ueda Y, Yamashita K, et al. Stem-like progenitor and terminally differentiated T_{FH}-like $CD4^+$ T cell exhaustion in the tumor microenvironment. Cell Rep 2024;43:113797.
12. Nagasaki J, Togashi Y. A variety of "exhausted" T cells in the tumor microenvironment. Int Immunol 2022;34:563–70.
13. Crotty S. T follicular helper cell biology: a decade of discovery and diseases. Immunity 2019;50:1132–48.
14. Lee SK, Rigby RJ, Zotos D, Tsai LM, Kawamoto S, Marshall JL, et al. B cell priming for extrafollicular antibody responses requires Bcl-6 expression by T cells. J Exp Med 2011;208:1377–88.
15. Weinstein JS, Herman EI, Lainez B, Licona-Limón P, Esplugues E, Flavell R, et al. TFH cells progressively differentiate to regulate the germinal center response. Nat Immunol 2016;17:1197–205.
16. Yusuf I, Kageyama R, Monticelli L, Johnston RJ, Ditoro D, Hansen K, et al. Germinal center T follicular helper cell IL-4 production is dependent on signaling lymphocytic activation molecule receptor (CD150). J Immunol 2010; 185:190–202.
17. Fridman WH, Meylan M, Petitprez F, Sun CM, Italiano A, Sautès-Fridman C. B cells and tertiary lymphoid structures as determinants of tumour immune contexture and clinical outcome. Nat Rev Clin Oncol 2022;19:441–57.
18. Schaerli P, Willimann K, Lang AB, Lipp M, Loetscher P, Moser B. CXC chemokine receptor 5 expression defines follicular homing T cells with B cell helper function. J Exp Med 2000;192:1553–62.
19. Breitfeld D, Ohl L, Kremmer E, Ellwart J, Sallusto F, Lipp M, et al. Follicular B helper T cells express CXC chemokine receptor 5, localize to B cell follicles, and support immunoglobulin production. J Exp Med 2000;192:1545–52.
20. Shi J, Hou S, Fang Q, Liu X, Liu X, Qi H. PD-1 controls follicular T helper cell positioning and function. Immunity 2018;49:264–74.e4.
21. Cui C, Wang J, Fagerberg E, Chen PM, Connolly KA, Damo M, et al. Neoantigen-driven B cell and CD4 T follicular helper cell collaboration promotes anti-tumor CD8 T cell responses. Cell 2021;184:6101–18.e13.
22. Ruggiu M, Guérin MV, Corre B, Bardou M, Alonso R, Russo E, et al. Anti-PD-1 therapy triggers Tfh cell-dependent IL-4 release to boost CD8 T cell responses in tumor-draining lymph nodes. J Exp Med 2024;221: e20232104.
23. Niogret J, Berger H, Rebe C, Mary R, Ballot E, Truntzer C, et al. Follicular helper-T cells restore $CD8^+$-dependent antitumor immunity and anti-PD-L1/PD-1 efficacy. J Immunother Cancer 2021;9:e002157.
24. Garaud S, Buisseret L, Solinas C, Gu-Trantien C, de Wind A, Van den Eynden G, et al. Tumor infiltrating B-cells signal functional humoral immune responses in breast cancer. JCI Insight 2019;5:e129641.
25. Gu-Trantien C, Loi S, Garaud S, Equeter C, Libin M, de Wind A, et al. $CD4^+$ follicular helper T cell infiltration predicts breast cancer survival. J Clin Invest 2013;123:2873–92.
26. Gutiérrez-Melo N, Baumjohann D. T follicular helper cells in cancer. Trends Cancer 2023;9:309–25.
27. Amé-Thomas P, Le Priol J, Yssel H, Caron G, Pangault C, Jean R, et al. Characterization of intratumoral follicular helper T cells in follicular lymphoma: role in the survival of malignant B cells. Leukemia 2012;26:1053–63.
28. Pandey S, Mourcin F, Marchand T, Nayar S, Guirriec M, Pangault C, et al. IL-4/CXCL12 loop is a key regulator of lymphoid stroma function in follicular lymphoma. Blood 2017;129:2507–18.
29. Amé-Thomas P, Hoeller S, Artchounin C, Misiak J, Braza MS, Jean R, et al. CD10 delineates a subset of human IL-4 producing follicular helper T cells involved in the survival of follicular lymphoma B cells. Blood 2015;125:2381–5.
30. Rawal S, Chu F, Zhang M, Park HJ, Nattamai D, Kannan S, et al. Cross talk between follicular Th cells and tumor cells in human follicular lymphoma promotes immune evasion in the tumor microenvironment. J Immunol 2013; 190:6681–93.
31. Pascutti MF, Jak M, Tromp JM, Derks IA, Remmerswaal EB, Thijssen R, et al. IL-21 and CD40L signals from autologous T cells can induce antigen-independent proliferation of CLL cells. Blood 2013;122:3010–9.
32. Norén GN, Orre R, Bate A, Edwards IR. Duplicate detection in adverse drug reaction surveillance. Data Mining Knowledge Discov 2007;14:305–28.
33. Bergvall T, Norén GN, Lindquist M. vigiGrade: a tool to identify well-documented individual case reports and highlight systematic data quality issues. Drug Saf 2014;37:65–77.
34. Gao X, Wang H, Chen Z, Zhou P, Yu D. An optimized method to differentiate mouse follicular helper T cells in vitro. Cell Mol Immunol 2020;17:779–81.
35. Kalmanti L, Saussele S, Lauseker M, Müller MC, Dietz CT, Heinrich L, et al. Safety and efficacy of imatinib in CML over a period of 10 years: data from the randomized CML-study IV. Leukemia 2015;29:1123–32.
36. Fine JP, Gray RJ. A proportional hazards model for the subdistribution of a competing risk. J Am Stat Assoc 1999;94:496–509.
37. Boudou-Rouquette P, Grignano E, Arrondeau J, Burroni B, Chouchana L. Diffuse large B-cell lymphoma after nivolumab treatment for lung cancer: a case report and a World Health Organization pharmacovigilance database review. Eur J Cancer 2020;130:20–2.
38. Francisco LM, Sage PT, Sharpe AH. The PD-1 pathway in tolerance and autoimmunity. Immunol Rev 2010;236:219–42.
39. Okazaki T, Maeda A, Nishimura H, Kurosaki T, Honjo T. PD-1 immunoreceptor inhibits B cell receptor-mediated signaling by recruiting src homology 2-domain-containing tyrosine phosphatase 2 to phosphotyrosine. Proc Natl Acad Sci U S A 2001;98:13866–71.
40. Xu-Monette ZY, Zhou J, Young KH. PD-1 expression and clinical PD-1 blockade in B-cell lymphomas. Blood 2018;131:68–83.
41. Snell LM, Xu W, Abd-Rabbo D, Boukhaled G, Guo M, Macleod BL, et al. Dynamic $CD4^+$ T cell heterogeneity defines subset-specific suppression and PD-L1-blockade-driven functional restoration in chronic infection. Nat Immunol 2021;22:1524–37.
42. Maceiras AR, Almeida SCP, Mariotti-Ferrandiz E, Chaara W, Jebbawi F, Six A, et al. T follicular helper and T follicular regulatory cells have different TCR specificity. Nat Commun 2017;8:15067.
43. Kim J, Lee H, Lee JE, Choi G, Chung H, Kim D, et al. Liver X receptor controls follicular helper T cell differentiation via repression of TCF-1. Proc Natl Acad Sci U S A 2023;120:e2213793120.
44. Chen S, Lee LF, Fisher TS, Jessen B, Elliott M, Evering W, et al. Combination of 4-1BB agonist and PD-1 antagonist promotes antitumor effector/memory CD8 T cells in a poorly immunogenic tumor model. Cancer Immunol Res 2015;3:149–60.
45. Polesso F, Munks MW, Rott KH, Smart S, Hill AB, Moran AE. PD-1-specific "Blocking" antibodies that deplete $PD\text{-}1^+$ T cells present an inconvenient variable in preclinical immunotherapy experiments. Eur J Immunol 2021;51: 1473–81.
46. van Eijs MJM, van der Wagen LE, Mous R, Leguit RJ, van de Corput L, van Lindert ASR, et al. Hematologic malignancies following immune checkpoint inhibition for solid tumors. Cancer Immunol Immunother 2023;72:249–55.

47. Laurent C, Dietrich S, Tarte K. Cell cross talk within the lymphoma tumor microenvironment: follicular lymphoma as a paradigm. Blood 2024;143: 1080–90.
48. Cerchietti L. Genetic mechanisms underlying tumor microenvironment composition and function in diffuse large B-cell lymphoma. Blood 2024;143: 1101–11.
49. Heudel PE, de Montfort A, Debieuvre D, Chouaid C, Carton M, Audigier-Valette C, et al. Reduced risk of secondary primary extra pulmonary cancer in advanced/metastatic lung cancer patients treated with immune checkpoint inhibitors. Lung Cancer 2023;182:107280.
50. Heudel P, Chabaud S, Perol D, Flechon A, Fayette J, Combemale P, et al. Immune checkpoint inhibitor treatment of a first cancer is associated with a decreased incidence of second primary cancer. ESMO Open 2021;6:100044.
51. Harrold EC, Foote MB, Rousseau B, Walch H, Kemel Y, Richards AL, et al. Neoplasia risk in patients with Lynch syndrome treated with immune checkpoint blockade. Nat Med 2023;29:2458–63.
52. Heudel P, Chabaud S, Perol D, Ray-Coquard I, Blay JY. Reduced risk of second primary cancer in patients treated with immune checkpoint inhibitors for a first cancer. Ann Oncol 2020;31:1773–5.
53. Goodman A, Patel SP, Kurzrock R. PD-1-PD-L1 immune-checkpoint blockade in B-cell lymphomas. Nat Rev Clin Oncol 2017;14:203–20.
54. Ansell SM, Lesokhin AM, Borrello I, Halwani A, Scott EC, Gutierrez M, et al. PD-1 blockade with nivolumab in relapsed or refractory Hodgkin's lymphoma. N Engl J Med 2015;372:311–9.
55. Lesokhin AM, Ansell SM, Armand P, Scott EC, Halwani A, Gutierrez M, et al. Nivolumab in patients with relapsed or refractory hematologic malignancy: preliminary results of a phase Ib study. J Clin Oncol 2016;34:2698–704.
56. Zinzani PL, Thieblemont C, Melnichenko V, Bouabdallah K, Walewski J, Majlis A, et al. Pembrolizumab in relapsed or refractory primary mediastinal large B-cell lymphoma: final analysis of KEYNOTE-170. Blood 2023;142: 141–5.
57. Armand P, Rodig S, Melnichenko V, Thieblemont C, Bouabdallah K, Tumyan G, et al. Pembrolizumab in relapsed or refractory primary mediastinal large B-cell lymphoma. J Clin Oncol 2019;37:3291–9.
58. Medeiros LJ, Chadburn A, Natkunam Y, Naresh KN; WHO 5th Edition Classification Project. Fifth edition of the World Health Classification of tumors of the hematopoietic and lymphoid tissues: B-cell neoplasms. Mod Pathol 2024;37:100441.
59. Ariyasu R, Kakuto S, Miyadera K, Akita T, Kiritani A, Tsugitomi R, et al. Real-world outcome analysis of patients with stage IV NSCLC treated with tyrosine kinase and immune checkpoint inhibitors. JTO Clin Res Rep 2023; 4:100524.
60. Wartewig T, Kurgyis Z, Keppler S, Pechloff K, Hameister E, Öllinger R, et al. PD-1 is a haploinsufficient suppressor of T cell lymphomagenesis. Nature 2017;552:121–5.
61. Wartewig T, Daniels J, Schulz M, Hameister E, Joshi A, Park J, et al. PD-1 instructs a tumor-suppressive metabolic program that restricts glycolysis and restrains AP-1 activity in T cell lymphoma. Nat Cancer 2023;4:1508–25.